This is an open access article published under an ACS AuthorChoice License, which permits copying and redistribution of the article or any adaptations for non-commercial purposes.

ACS OMEGA

http://pubs.acs.org/journal/acsodf

Article

Nanohydroxyapatite-, Gelatin-, and Acrylic Acid-Based Novel Dental Restorative Material

Kashma Sharma, Shreya Sharma, Sonia Thapa, Madhulika Bhagat, Vijay Kumar,* and Vishal Sharma*

Cite This: *ACS Omega* 2020, 5, 27886−27895

Read Online

ACCESS | Metrics & More | Article Recommendations

ABSTRACT: The aim of this study was to prepare a novel dental restorative material (NDRM) and to understand its cell viability behavior. The hydroxyapatite (HA) nanopowder was synthesized using a wet chemical precipitation method using calcium hydroxide and orthophosphoric acid as precursors. The as-prepared HA nanopowder was annealed at different temperatures to get a pure compound with a Ca/P ratio close to 1.67. The optimal temperature was found to be 600 °C, whereas at a higher temperature, HA starts decomposing into CaO. The preparation of NDRM was conducted in two steps. The first step comprises the preparation of HA nanopowder- and gelatin (G)-based film using microwave heating. In the second step, the homogenized mixture of the HA-G film was mixed with different amounts of acrylic acid to form a self-flowable NDRM paste. Further, both these materials (HA nanopowder and NDRM) were characterized using FTIR, XRD, and SEM−EDX analyses. The FTIR and XRD results show the peaks corresponding to natural bone apatite and therefore confirm the formation of HA. EDX results showed the presence of Ca and P in HA nanopowder and NDRM with Ca/P ratios of 1.79 and 1.63, respectively. Synthesized NDRM was also analyzed for its *in vitro* cytotoxic and reproductive viability potential against normal cells using MTT and clonogenic assay. The analysis showed significantly higher cellular viability on the treatment with NDRM when compared to HA nanopowder as well as no colony suppression by both materials was observed on the normal cell line (fR2) even after exposure for 24 h, indicating its nontoxicity. The synthesized NDRM therefore can be considered as a promising candidate for dental caries restoration applications.

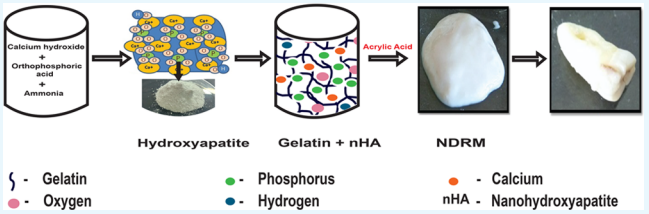

1. INTRODUCTION

In today's scenario, dental problems such as dental caries, cavities, rotting teeth, etc., are widespread chronic diseases that affect millions of people around the globe.[1−5] Various factors are responsible for dental caries, for instance, high starch, poor oral cleanliness, less consumption of water, boron inadequacy, consumption of highly acidic food and beverages, etc.[2] Moreover, preservatives and junk food generally enhanced the use of dietary acids, culminating in unnecessary intake of acidic drinks within our modern culture, which is also one of the factors.[5] This transformation in the human diet also affected the oral ecosystem and resulted in various dental problems (dental caries and tooth decay) along with other diseases.[6−8] Dental caries are permanent; existing medical treatment and materials cannot make the body naturally heal from a dental infection.[2] The technique to cure the microbial disease that is responsible for the demolition of the teeth is normally to expel cavities or rotting teeth by a doctor. At that point, a dental filling is mandatory to fix the teeth.

Hydroxyapatite (HA; $Ca_{10}(PO_4)_6(OH)_2$), the essential mineral part of the human bones and teeth, is considered as the main research problem prompting the enhancement of properties and novel applications of biomaterials in various sectors of biomedical science and technology.[9−15] It shows properties like biocompatibility, bioactivity, chemical and structural resemblance with the mineral phase of bone and dental tissue, bonding with the host material, osteoconductivity, and the absence of inflammatory response, empowering its tissue engineering applications.[14−16] HA is employed in the orthopedic, dental, and maxillofacial medical procedures as a bone replacement, which is due to its structural similarity to bone mineral and can be used in coatings for hip substitutions and bone implanting materials.[17−19]

Various improvements in bioactive ceramics comprising calcium phosphates and HA occurred during the 1980s.[20] Thereafter, HA has been continuously used in grafts for immediate and quick bonding to living bone tissue. Calcium phosphate cement (CPC) was revealed to have the potential for various dental applications.[21−28] Domingo et al.[29] studied the hydrolytic balance of experimental HA-filled dental composite materials and suggested that more experiments are needed to enhance the interplay of nHA with the polymer

Received: June 29, 2020
Accepted: October 13, 2020
Published: October 22, 2020

© 2020 American Chemical Society

https://dx.doi.org/10.1021/acsomega.0c03125
ACS Omega 2020, 5, 27886−27895

matrix, which will permit the enhancement of the total loading of reinforcing filler, and subsequently to enhance the mechanical properties. During the subsequent year, Blind et al.[21] deposited thin films of HA on different substrates by a pulse laser deposition method. Bryington et al.[30] recommended that the HA nanopowder coating has a greater effect on the bone curing process in initial curing phases and the impact of microtopography is more effective at totally recovered phases. Additional examinations are required from various viewpoints to explain the role of bioactive coatings. Tschoppe et al.[31] investigated the impact of HA nanopowder toothpaste on remineralization of bovine enamel and dentine subsurface lesions and pointed out that HA nanopowder exhibited higher remineralizing effects in comparison to amine fluoride toothpaste with bovine dentine. The impact of HA nanopowder was checked on remineralization of tooth enamel by Nozari and fellow scientists by studying the capability of NaF varnish, HA nanopowder, and nanosilver fluoride in the enamel of primary anterior teeth.[32]

In our earlier work, we demonstrated the development of a gold nanoparticle (AuNP)-impregnated HA nanocomposite to accelerate the adsorption of methylene blue dye from wastewater.[33] The dye adsorbed waste material has also been used as an effective antibacterial agent. Herein, a novel dental restorative material (NDRM) was prepared using HA nanopowder, gelatin (G), and acrylic acid. Gelatin is one of the most common natural biopolymers for biomedical applications. Gelatin has various advantages like cell adhesive structure, cheaper cost, off-the-shelf availability, high biocompatibility, biodegradability, and low immunogenicity.[34] HA nanopowder combined with gelatin to form bionanocomposites has been prepared for studying periodontal tissue engineering scaffolds.[35] Dressler et al.[36] also investigated the effect of various parameters on the mechanical properties of the gelatin-coated porous ceramics. Hydrogels are widely used in the pharmaceutical and biomedical applications.[37,38] Physicochemical and biological properties of hydrogel/gelatin/hydroxyapatite PAA/G/HAp/AgNPs composites modified with silver nanoparticles were reported by Sobczak-Kupiec and co-workers.[39]

In this work, an effort has been put to prepare an NDRM primarily based on HA nanopowder, gelatin, and acrylic acid. The main aim was to determine its chemical compositions and to study the effect of different concentrations of HA nanopowder and NDRM on cell viability and cell survival using MTT and clonogenic assay. Additionally, the effects of physical properties such as washout resistance with hot and cold treatment along with the effect of different pH values were also studied to explore the possibility of mimicking the conventional dental filling material. To the best of the author's survey of the literature, the application of dental inserts based on nHA, gelatin, and acrylic acid as an NDRM has not been explored before.

2. RESULTS AND DISCUSSION

HA nanopowder was prepared *via* a wet precipitation method using calcium and phosphate ions as precursors, maintaining its stoichiometric Ca/P ratio close to 1.67.[35] To obtain the required Ca/P ratio, the initial reaction of water and calcium oxide was carried out at a pH 12.86; after maturation of the reaction, orthophosphoric acid was further added at a slightly acidic (pH 6.87) condition. Thereafter, the reaction mixture was turned basic by adding up ammonia, resulting in the formation of HA nanopowder with 1.79 Ca/P ratio at an optimum temperature of 600 °C. Additionally, the obtained HA nanopowder appears to be white in color with high crystallinity, suggesting the presence of more calcium ions, making this method comparatively more advantageous and simple. As indicated by various cited literature to boost bone regeneration, it is crucial to apply a sufficient Ca/P ratio to the ceramic material that encourages natural bone growth. The number of calcium ions and phosphate ions necessary for precipitation enhanced the shape, bioactivity, biocompatibility, and strength, making it efficient for enamel implants.[40] The effect of mineralization was enhanced by nanosize preparation and deposition to tooth enamel. The preparation of hydroxyapatite was done according to the following reactions given below.[40]

$$CaO + H_2O \rightarrow Ca(OH)_2 \quad (1)$$

$$10Ca(OH)_2 + 6H_3PO_4 \rightarrow Ca_{10}(PO_4)_6(OH)_2 + 18H_2O \quad (2)$$

A novel dental restorative material was successfully synthesized by the incorporation of HA nanopowder in the gelatin matrix through microwave heating *via* a three-step synthesis method. In the first step, the HA powders get dispersed or well mixed with gelatin (G) solution with continuous stirring, resulting in the formation of the HA-G matrix.[35] Gelatin is negatively charged at neutral pH, while HA exhibits amphoteric nature. The amphoteric structure of HA provides a number of active sites for gelatin molecules to form strong H-bonding with the H−OH group of HA-G nanocomposite.[41] The nitrogen atom of the gelatin molecules interacts with Ca^{2+} groups of HA *via* Lewis acid−base interaction.[42] The combination of HA nanopowder and gelatin is likely to give enhanced properties to this paste both from biological and mechanical perspectives. It was documented in the literature that the addition of gelatin into the HA matrix increases the HA strength by bridging the material cracks.[35,43]

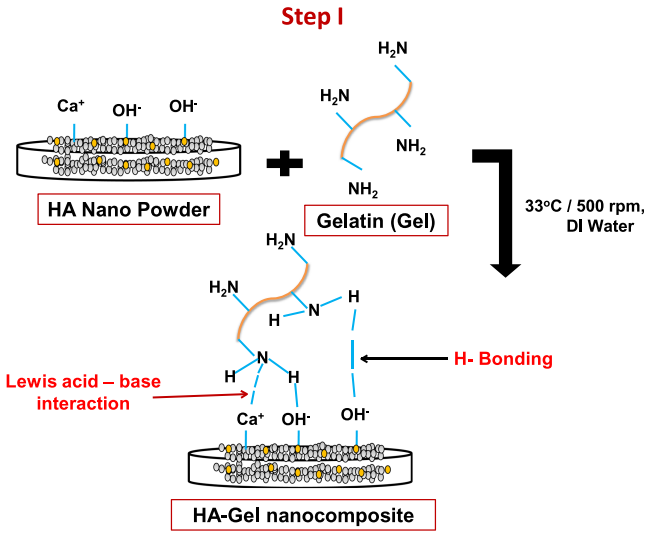

In the second step, the self-ionization process of water molecules helps in the generation of hydroxyl ion radicals. In the ionization process, H_2O molecules deprotonate to become an OH^- ion. The hydrogen nucleus (H^+) instantly protonates one more H_2O molecule to form H_3O^+ ions. H_2O molecules in the presence of heat get to break down in H^+ and hydroxyl radical (−OH*) moieties.[44] The −OH* radical is the neutral form of −OH ion and is a very reactive free radical.[45]

https://dx.doi.org/10.1021/acsomega.0c03125
ACS Omega 2020, 5, 27886−27895

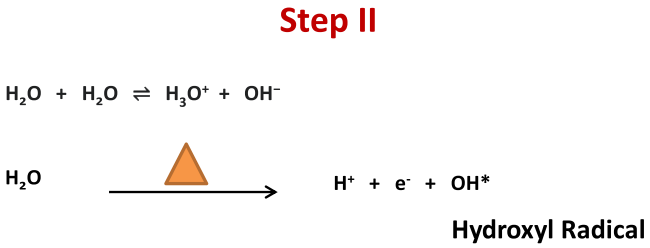

The formed HA-G nanocomposite was crushed and this leads to disruption of the network structure of the gel. Thereafter, it polymerizes with acrylic acid with constant stirring. The polymerization between acrylic acid and gelatin produced a quite stretchable and flowable paste due to heat treatment-induced permanent softening of the gel.[46] In the third step, the free radical initiates the generation of active sites over the composite and an acid surface for polymerization. The —C═O group of acrylic acid has H-bonding interaction with the $-NH_2$ group of HA/gel nanocomposite. Carboxylic acids and amide groups show an intermolecular hydrogen bonding in H_2O, and methyl groups of poly(acrylic acid) stabilize the hydrogen bonds.[46−48] This interaction results in the formation of NDRM paste.

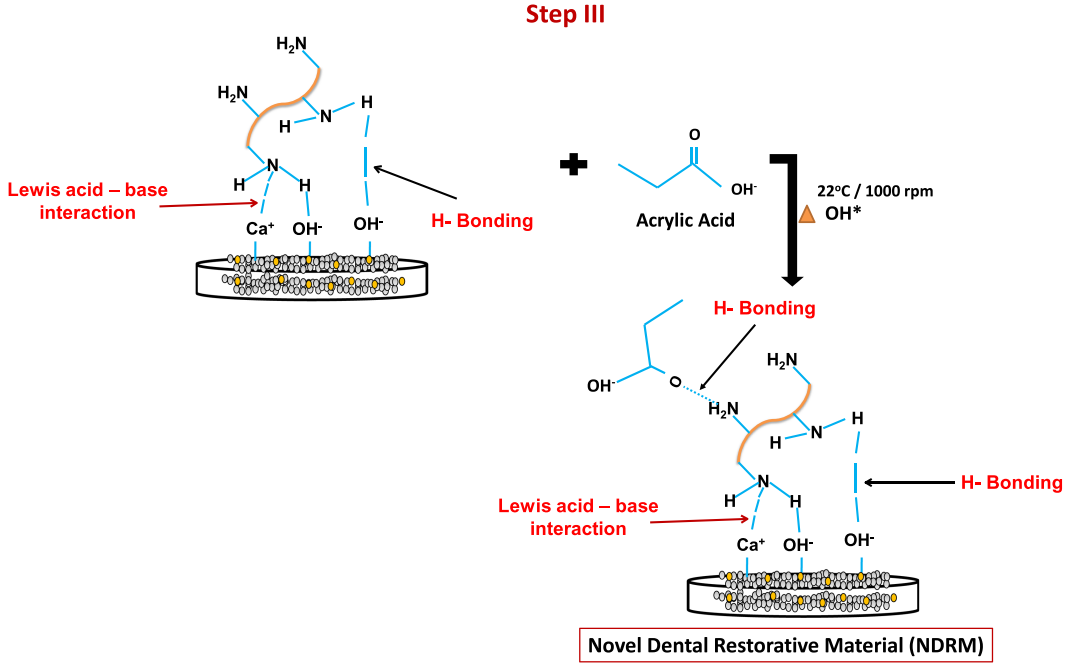

The amount of acrylic acid was varied from 0.5 to 2.5 mL to get the best homogenized self-flowable paste superficially. The amount less than the optimized value was not able to mix well with the HA-G nanopowder to give it a self-flowable nature. Meanwhile, a further increase in acrylic acid leads to self-cross-linking and results in an excessive sticky material (Figure 1). The synthesized HA-G-AA, *i.e.*, NDRM with 1 mL of acrylic acid, imparts the same morphology as observed in the case of enamel and turns hard on drying at 40 °C for 24 h. The formed composite appeared white, comparatively had a hard surface, and properly adhered to the void to fill it completely. The presence of HA nanopowder and gelatin in the composite provided the required amount of hardness, strength, and biocompatibility. Additionally, the incorporation of acrylic acid provides antiadhesive properties on plaque accumulation and enamel demineralization in low-caries adolescents.[49] Fornell and co-workers[50] employed antiadhesive polymeric enamel coating in combination with orthodontic appliances in adolescents with low caries cases and found no clinical effects. It had been suggested that the incorporation of a polymer such as acrylic acid into ceramic materials provides flexibility to the paste and helps bind with the enamel. In a study, Peroglio and co-workers[51] reported the hardening of bioceramic scaffolds by using a polymer coating and concluded that such a method may also be appropriate in comparison to other ceramic materials. Thus, these materials can possibly be used as a synthetic bone substitute for load-bearing applications without the help of invasive fixation devices.

2.1. Morphology of the nHA and NDRM. SEM images of HA nanopowder and NDRM are represented in Figure 2. The prepared HA nanopowder showed a cluster-like morphology that may contain many fine particles (Figure 2a).[33] The images also indicated a nonspherical shape, porous structure, and angular appearance with a rough surface. At a higher magnification, the HA nanopowder surface shows a clear cluster of small particles. On the other hand, SEM images of the modified composite by the addition of gelatin and acrylic acid showed agglomerated clusters of spherical-shaped granular appearance (Figure 2b). NDRM exhibits high porosity, which may be due to bonding between acrylic acid and gelatin molecules with HA nanopowder. Many studies reported that granules with an even spherical morphology have a straightforward structural and functional similarity with living bone tissues that improve osseointegration.[52,53]

The presence of Ca, P, and O within the crystallite was ascertained by EDX results (not shown). EDX analysis of HA nanopowder and NDRM shows the presence of Ca, P, and O within the crystallites, representing the formation of HA nanopowder-based materials. The spectrum of HA nanopowder depicts the presence of calcium and phosphorus in a very high quantity, which can also be seen in the corresponding values found during EDX analysis. The calculated atomic percentage of Ca/P ratios for HA nano-

https://dx.doi.org/10.1021/acsomega.0c03125
ACS Omega 2020, 5, 27886−27895

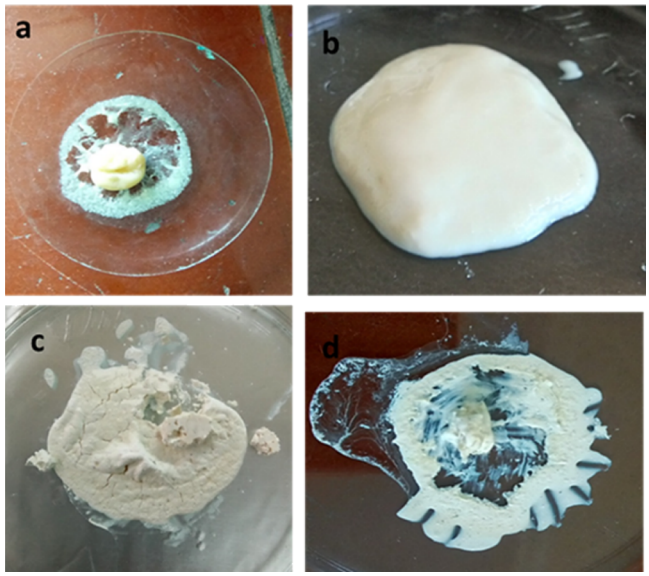

Figure 1. Preparation of the novel dental restorative material (NDRM): (a) HA + gelatin powder in 0.5 mL of AA, (b) HA + gelatin powder in 1 mL of AA, (c) HA + gelatin powder in 1.5 mL of AA, and (d) HA + gelatin powder in 2 mL of AA.

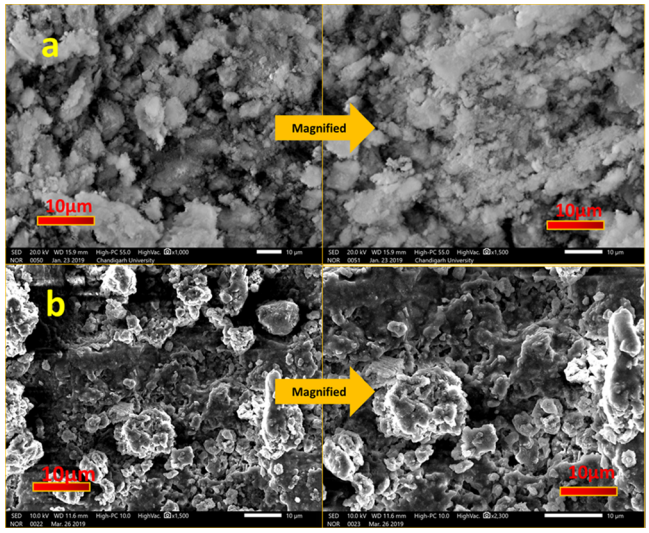

Figure 2. SEM images of (a) nanohydroxyapatite and (b) NDRM.

powder was found to be around 1.79. This is analogous to the ideal stoichiometric Ca/P ratio of HA (1.67).[54] The calculated Ca/P ratio for NDRM was calculated to be 1.63. The incorporation of acrylic acid and gelatin causes a decrease in atomic percentages of calcium ions and phosphate ion (Ca/P = 1.63) due to the bonding phenomenon. Comparatively, the Ca/P ratio (1.63) of NDRM appeared to be the closest to the stoichiometric Ca/P ratio of HA (1.67).[54] It is clear from the literature that to boost bone regeneration, it is crucial to apply enough Ca/P ceramic material that encourages natural bone growth. The number of calcium ions and phosphate ions is necessary for precipitation, enhancing the shape and its bioactivity, biocompatibility, and strength, which makes it efficient for enamel implants.[36] The EDX study also showed the formation of apatite by detecting Ca/P ratios very close to 1.67.[54]

2.2. XRD and FTIR Analysis. The XRD patterns of HA annealed at different temperatures and NDRM are displayed Figure 3. The diffraction peaks of HA were indexed to the

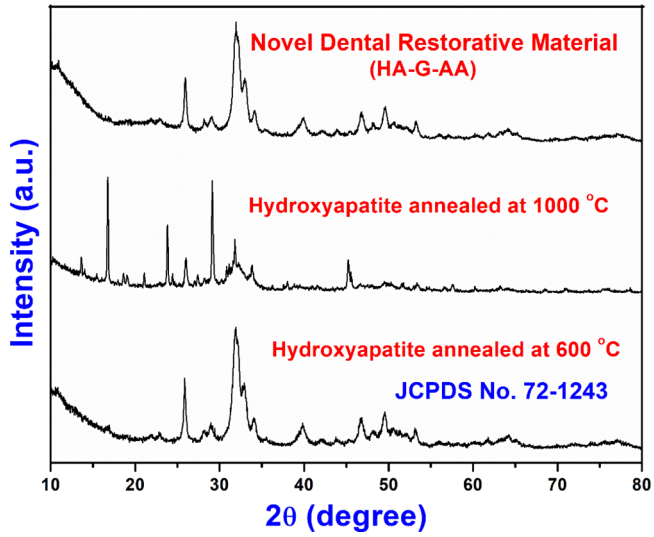

Figure 3. XRD patterns of nHA (annealed at 600 and 1000 °C) and NDRM.

hexagonal structure of HA with space group $P63/m$.[33] The diffraction peaks of HA are in accordance with JCPDS no. 72-1243.[33] It was seen that HA powder annealed at 600 °C imparts pure HA powder, while HA annealed at 1000 °C showed peaks with low intensity and reduction in crystalline nature. The average crystallite size of HA powder was found to be around 18.43 nm. Therefore, we have considered HA annealed at 600 °C for further studies. It was interesting to note that the intensity of the diffraction peaks increased with cross-linking of acrylic acid and gelatin over the synthesized HA nanopowder, which showed improvement in crystallinity. This may be due to the interaction of gelatin and acrylic acid chains with the HA nanopowder matrix.[55] This behavior can also be correlated with the change in surface morphology as clear from the SEM images.

FTIR spectroscopy was performed to look at the functional groups present in HA nanopowder and NDRM (Figure 4). The complete analysis of functional groups present in HA nanopowder annealed at 600 °C was carried out as discussed earlier (Figure 4a).[33] The FTIR spectrum of HA nanopowder shows clear bands in the wavenumber range of 1040−560 cm^{-1}, which are features for the phosphate of the HA phase. The sharp peak at 563 cm^{-1} and a small peak around 509 cm^{-1} are attributed to the bending mode of O−P−O.[56] The small band at 1454 cm^{-1} may be attributed to the carboxylate group coordinated to the HA surface under different configurations.[56] A sharp peak was observed at 1028 cm^{-1}, which may be credited to the asymmetric stretching of phosphate ions (PO_4^{3-}).[57] The mixture of HA nanopowder, gelatin, and acrylic acid shows major peaks of HA nanopowder, gelatin, and acrylic acid. The FTIR spectrum of NDRM (Figure 4b) showed that peaks at 1637 and 1538 cm^{-1} may be attributed to acylamino I and acylamino II, respectively.[58] The other peaks at 1300−1000 and 540−510 cm^{-1} may be credited to C−O stretching vibration and C═O bending vibration of ketone, respectively. The peak detected at 1551 cm^{-1} relates to aliphatic C═C and carbonyl C═O groups.[59] The peak at

https://dx.doi.org/10.1021/acsomega.0c03125
ACS Omega 2020, 5, 27886−27895

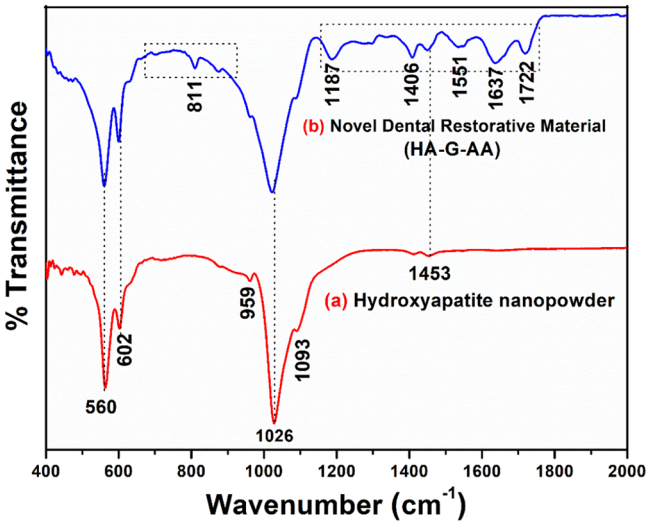

Figure 4. FTIR spectra of (a) hydroxyapatite nanopowder and (b) NDRM.

1637 cm^{-1} corresponds to the —C═O antisymmetric stretching band of the carboxylate groups in poly(acrylic acid)[60] and confirms the attachment of acrylic acid chains over HA nanopowder with gelatin.

2.3. Effect of Hot and Cold Treatment and Acidity over Synthesized NDRM. Acidity or low pH leads to demineralization in tooth enamel, leading to tooth decay and caries. Because of higher acid production or more basicity, enamel may deteriorate with time and thus cause loss of mineralization activity. Demineralization occurs due to sticky and sweet food products, bacteria, and narrow use of shielding agents found in fluoride, salivary buffers, and antimicrobial agents. Demineralization arises at a low pH when the oral environment is undersaturated with mineral ions, relative to a tooth's mineral content.[61] The pH present in the mouth of a human is around 6.8. Saliva present in the mouth may affect the loss of mineral by certain tooth whiteners due to the release of components such as hydrogen carbonate, calcium fluoride, and hydrogen phosphate. These are important to keep up a balance between demineralization and remineralization.[62] We have studied the impact of pH and temperature over prepared NDRM. The prepared NDRM was subjected to various pH conditions up to 6 h. It was observed that the NDRM kept in a pH 4 solution showed a 0.0016 g weight loss. On the other hand, the NDRM kept in a solution of pH 7 showed a 0.001 g weight loss, whereas a 0.002 g weight loss was observed in NDRM kept in a solution of pH 9. The weight loss observed was quite insignificant (Table 1). Interestingly, no weight loss was detected in NDRM kept in hot and cold water (Figure 5 and Table 2). This may be due to the fact that the hybrid assembly of gelatin and HA nanopowder is likely to provide enhanced properties of the scaffold from the biological and mechanical perspectives.[36] Second, HA nanopowder is a good source of free Ca, and this is essential for the defense

Table 1. pH Studies of NDRM

pH of solution	initial weight (g)	final weight (g)	percentage weight loss
pH 4	1.5738	1.5722	0.1%
pH 7.5	1.6553	1.6518	0.06%
pH 9	3.0801	3.0534	0.8%

Figure 5. Washout resistance test of NDRM in hot and cold water.

Table 2. Treatment of Hot and Cold Water of NDRM

condition	initial weight (g)	final weight (g)	percentage weight loss
hot water	1.6262	1.6230	0.1%
cold water	0.7807	0.7759	0.6%

from dental caries and erosion. The prevention of dental erosion can be increased with an increase in the concentration of HA nanopowder.

2.4. Evaluation of Cytotoxicity Using MTT Assay. *In vitro* cytotoxicity potential of nanohydroxyapatite and NDRM was studied against the normal human breast epithelial cell line (fR2) using MTT assay. Colorimetric analysis using tetrazolium salt MTT (3-(4,5-dimethylthiazol-2-yl)-2,5-diphenyltetrazolium bromide) was employed to find the viability of cells, which interacted with various concentrations of nHA and NDRM. Significantly lower cytotoxicity was observed when treated with different HA nanopowder concentrations (Table 3). Likewise, NDRM also showed very low cytotoxicity at 100

Table 3. *In Vitro* Cytotoxic Potential of HA Nanopowder and NDRM against Normal Human Breast Epithelial Cells (fR2)

concentration (μg)	% inhibition (HA nanopowder)	% inhibition (NDRM)	IC_{50}
5	0	0	>100 μg
10	0	0	
30	4.90 ± 1.97	0	
50	7.81 ± 3.46	0	
100	13.70 ± 1.09	3.1 ± 0.5	
200	17.06 ± 1.8	13.6 ± 0.5	

and 200 μg against the fR2 cell line. The results showed that cell growth and proliferation were not inhibited by the HA nanopowder slurry or NDRM against normal cell lines, which hence proved to be more compatible as desired (Table 3). The cell viability was concentration-dependent and was demonstrated as a percentage inhibition over the untreated control. This result was in accordance with the previous study of osteoblast response to HA nanopowder in other concentration ranges.[63,64] The nontoxic nature of the NDRM toward the FR2 cell line may be due to the fact that the NDRM with gelatin and acrylic acid had a smooth and well-constructed open-spaced porous structure, which exhibited more favorable cell viability and cell proliferation behavior, as depicted in the SEM images.[65]

2.5. Cell Growth and Colony Suppression by Given Compounds. Further, cell viability, as well as noncytotoxicity of nanohydroxyapatite and NDRM, was confirmed by observing their response to the normal fR2 cell line (normal

https://dx.doi.org/10.1021/acsomega.0c03125
ACS Omega 2020, 5, 27886−27895

breast epithelial cells) (Figure 6). Results indicated little morphological differences as compared to untreated cells

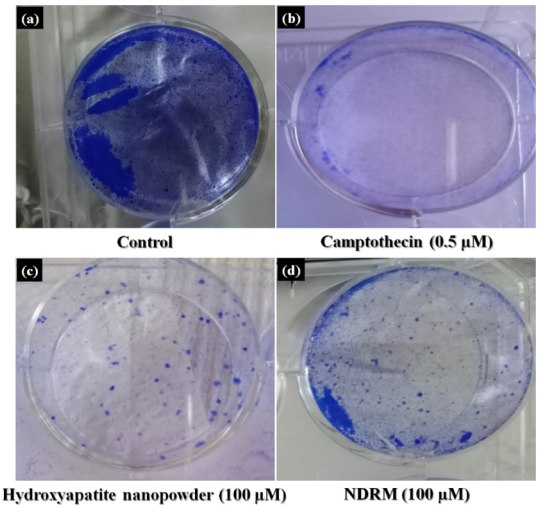

Figure 6. Effect of NDRM on the colony formation against normal breast epithelial cells (fR2): (a) control, (b) camptothecin, (c) hydroxyapatite nanopowder, and (d) NDRM.

(Figure 6a) and it was clear from the figure that the given compounds are nontoxic to the normal breast epithelial cell line and there is no colony suppression by the given compounds. Moreover, cell numbers were significantly reduced on exposure to positive control camptothecin at 0.1 μM as depicted in Figure 6b, whereas the cell number observed was higher in the case of NDRM as compared to nHA (Figure 6c), indicating the cell survival and viability of normal cells on treatments. Colony formation was reported as an *in vitro* quantitative technique to look at the potential of a single cell to grow into a large colony through clonal expansion.[66] This assay also measures cell survival, and it is normally employed as a sensitive model for measuring long-term cytotoxicity. Tests measuring metabolic death are short-term assays for measuring cell growth within 2 to 3 days of drug exposure, but clonogenic assays remain essential for the evaluation of the long-term cytotoxicity of drugs, which causes reversible growth inhibition.[66,67] Taken collectively, the data acquired from the viability tests suggest that nanohydroxyapatite and NDRM are not cytotoxic to normal cell lines.

Cellular morphology and adhesion properties on the NDRM were accredited to well-constructed open-spaced porous structures that give a bigger space for cell movement and surface area for cell attachment. Here, the SEM images show a porous and rough structure of HA nanopowder and porous and smooth morphology of NDRM. In addition, the HA nanoparticles can expand the initial attachment of the cells.[65,68] The preliminary binding of the cells mainly depends on the binding of adhesion molecules and their resulting mediation among the cells and the tested sample surface.[40,43,69] Second, the rough surface of HA nanopowder particles retards the cell proliferation rate, which was described in other systems,[70−72] whereas NDRM has pure gelatin and acrylate involved that give it a smooth and well-constructed open-spaced porous surface, resulting in a more promising cell proliferation behavior, as shown in Figure 6d.

The treatment of nanohydroxyapatite and NDRM, each at higher concentration (100 μM), on the fR2 cells results in viable colonies as compared to that of camptothecin (0.5 μM). However, when compared to the control, we observed less number of viable colonies (Figure 7). Therefore, we concluded

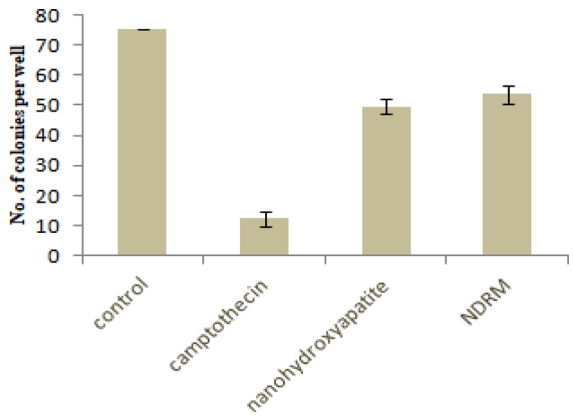

Figure 7. Effect of NDRM on the colony formation against normal breast epithelial cells (fR2).

that even at higher concentrations, molecules behave as less toxic to the normal cells. This indication of the differential effect on normal cells indicates the nontoxic nature of compounds as it increases the reproducibility and survival rates.

3. CONCLUSIONS

We have successfully prepared a novel dental restorative material as an alternative to the conventional materials for tooth-restoring applications. The wet precipitation method proves effective in the preparation of nanohydroxyapatite. The formation of the prepared nanohydroxyapatite and NDRM was confirmed through XRD and FTIR analyses. The characteristic FTIR peaks of different functional groups mark the presence of carbonate and phosphate ions, which was also supported by EDX analysis. The pH and hot and cold water studies showed that the dental filling material has a great capacity to withstand the acidic and basic environments as well as hot and cold conditions. The *in vitro* results from cell viability and cell survival against normal cells depicted nontoxic nature and showed that our compounds HA nanopowder and NDRM can be considered as safe. In other words, molecules provide a favorable microenvironment for the growth of cells. Hence, it can be a better alternative to be used as a promising dental restorative material in the dentistry area.

4. MATERIALS AND METHODS

4.1. Materials. Calcium oxide powder, orthophosphoric acid (H_3PO_4), ammonia solution, and hydrochloric acid were purchased from Sisco Research Laboratories Pvt. Ltd. (SRL), gelatin was purchased from Loba Chemie Pvt. Ltd., and acrylic acid was purchased from Central Drug House Pvt. Ltd. All were of analytical grade.

4.2. Preparation of Hydroxyapatite Nanopowder. Hydroxyapatite (HA) nanopowders were prepared through the well-known wet chemical precipitation method. The detailed synthesis procedure for the HA nanopowder is reported in our earlier work.[33] The different steps involved in the synthesis of HA nanopowder are depicted in Scheme 1.

4.3. Preparation of the Novel Dental Restorative Material (NDRM). The preparation of the paste is carried out

https://dx.doi.org/10.1021/acsomega.0c03125
ACS Omega 2020, 5, 27886−27895

Scheme 1. Various Steps Involved in the Synthesis of HA Nanopowder[a]

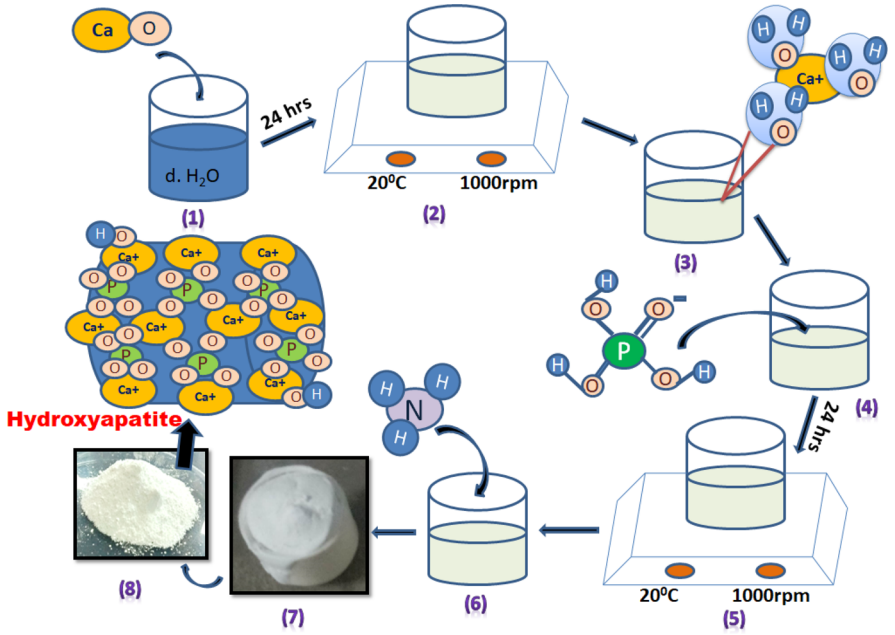

[a](1, 2) Mixing of CaO with dH_2O molecules, (3) interaction of calcium with bonded water, which is then removed, leaving bare Ca ions, (4, 5) ionic reaction of Ca with PO_4 and −OH ions, (6) addition of NH_3, and (7, 8) calcination of the synthesized material.

Scheme 2. Schematic Representation for the Preparation of Novel Dental Restorative Material (NDRM)[a]

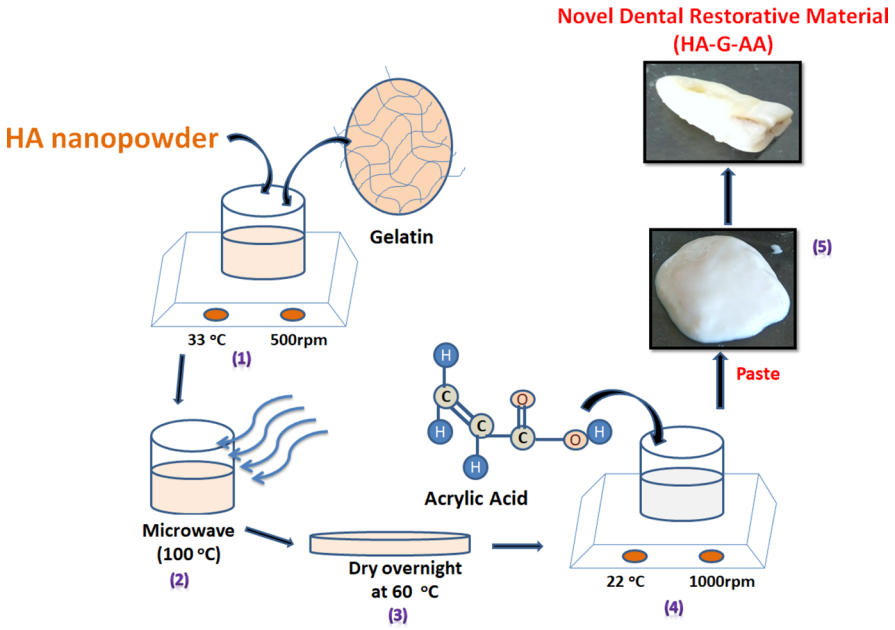

[a](1) Mixing of nanohydroxyapatite and gelatin, (2) microwave-assisted reaction, (3) obtained mixture in a Petri plate, (4) mixing of acrylic acid to the powder mixture, and (5) obtained NDRM self-flowable paste.

in two steps. In step 1, gelatin and HA nanopowder were taken in 1:2 ratios and added to a glass beaker containing 30 mL of distilled water with continuous stirring (1000 RPM), maintained at room temperature for 60 min. After complete mixing, the solution is kept in the microwave up to boiling (240 s). The resultant mixture was then transferred into a Petri dish and kept in a hot air oven for overnight drying at 60 °C. After drying, it becomes a film of nanohydroxyapatite and gelatin (nHA-gl). It is homogenized using mortar and pestle. One gram of the homogenized mixture was taken and then added to a glass beaker containing acrylic acid with constant stirring (1000 RPM) at 25 °C temperature, which is maintained using a temperature probe (Scheme 2). The amount of acrylic acid is varied from 0.5 to 2.5 mL to get the best homogenized self-flowable paste. After 20 min of stirring, it forms a sticky paste. This NDRM paste is then used to fill cavities of broken or eroded teeth.

4.4. Effect of Hot and Cold Water Treatment and Acidity over Synthesized NDRM. The washout resistance and sensitivity of NDRM were checked by keeping the tooth

https://dx.doi.org/10.1021/acsomega.0c03125
ACS Omega 2020, 5, 27886−27895

filled with NDRM in hot and cold water. The temperature of hot water was maintained at 100 °C and, for cold water, at 4 °C. The prepared NDRM was allowed to dip in both the hot and cold water for 6 h and further observed for the results.

To study the effect of pH on the NDRM or dental filling material, three pH solutions (4, 7.5, and 9) were maintained using dilute HCl and aqueous sodium hydroxide solution. The prepared NDRM-filled tooth was weighed initially before treatment and kept in the respective pH solution for 6 h. Over 6 h, teeth were dried and weighed again to note any significant change in weight loss. The percentage weight loss is calculated by the following formula

$$\text{percentage weight loss} = \frac{(\text{initial weight} - \text{final weight})}{\text{initial weight}} \times 100 \quad (3)$$

4.5. Characterization. Phase analysis was carried out by employing a Spinner PW3064 X'Pert PRO diffractometer with Cu-Kα of 0.154056 nm for a wide range of Bragg's angle 2θ ($10 < \theta < 80$) at the scanning rate of 1° per minute. The operating voltage and current for an X-ray gun are 40 kV and 40 mA, respectively. The average crystallite size (D) of the HA nanopowder was evaluated from the acquired XRD data by using the Scherrer formula.[59] The FTIR spectra of HA nanopowder and NDRM samples were recorded in transmission mode within the spectral range from 400 to 2000 cm^{-1} using an FTIR spectrophotometer (PerkinElmer) containing a diamond crystal and ZnSe for focusing element. The surface morphology of the prepared samples was determined by SEM (JEOL JSM-6490LV). Before the measurement, the samples were dried in air and sputter-coated with gold. A microwave oven 17PM-MECI (IFB) having a power source of 230 V and 50 Hz, with a frequency of 2450 MHz, was employed for intermediate steps.

4.6. Cell Culture and Growth Conditions. The normal human breast epithelial cell line (fR2) was obtained from the European Collection of Authenticated Cell Cultures (ECACC), U.K. The cell line was developed in tissue culture flasks in complete growth medium (RPMI-1640) enhanced with 10% fetal bovine serum, 100 mμ/mL streptomycin, and 100 units/mL penicillin (New Brunswick, Galaxy 170R, Eppendorf) at 37 °C in a humidified incubator with 5% CO_2.[72,73]

4.7. Cytotoxicity Assay (MTT Assay). In general, the viability of cells was estimated by MTT assay.[73] This assay identifies the reduction of MTT [3-(4,5-dimethylthiazolyl)-2,5-diphenyl-tetrazolium bromide] (Sigma) (a colorimetric technique) by mitochondrial dehydrogenase to a purple formazan product, which reflects the normal function of mitochondria and, hence, the measurement of cytotoxicity cell and viability. Briefly, an optimum cell density of 1×10^4 viable cells/well was seeded in 96-well flat-bottom plates in complete culture media (CCM). After 24 h of incubation under culture conditions, the cells were exposed to various concentrations (5, 10, 30, 50,100, and 200 μg/mL) of studied samples comprising a complete growth medium. The plates were retained under incubation under similar conditions for 24 h at 37 °C. Further, the cells were incubated with MTT (250 μg/mL in Dulbecco's PBS) at 37 °C for 4 h. DMSO was used to dissolve the formazan produced. The resulting colored solution was quantified by estimating the absorbance at 570 nm using a microplate reader (Bio-Rad ELISA Plate Reader) and IC_{50} was determined by using GraphPad Prism Software version 5.0. Experiments were executed in triplicate and results were expressed as mean ± SE. The percentage cell viability of fR2 cells was calculated using the following formula.[69,73]

$$\text{cell viability} = \frac{OD_{(\text{treated})}}{OD_{(\text{control})}} \times 100 \quad (4)$$

The percentage cell cytotoxicity was calculated as

$$\text{cytotoxicity} = 100 - \left[\frac{OD_{(\text{treated})}}{OD_{(\text{control})}} \times 100\right] \quad (5)$$

where $OD_{control}$ is the optical density of untreated cells, and $OD_{treated}$ is the optical density of cells treated with extract and fractions.

4.8. Colony Formation Assay. The human breast epithelial cell line (fR2) was treated with nHA and NDRM, each at 100 μM for 24 h. Cells were grown in complete growth medium in six-well plates. After 24 h, cells were treated with nHA and NDRM, each at 100 μM, and kept in an incubator at 37 °C for further 24 h. Camptothecin (0.5 μM) and media comprising 0.5% DMSO were employed as the positive and negative control, respectively. After 24 h of treatment, the old medium was aspirated; cells were washed twice with PBS, trypsinized, pelleted, resuspended in fresh medium, and counted. The cells in single suspension were plated with the density of 1000 to 2000 cells/well in six-well plates to allow the formation of the attached colonies. On the 7th day, the cells were fixed with 4% paraformaldehyde and stained with 0.4% crystal violet for 30 min at room temperature. Last, crystal violet was removed cautiously and washed with water. Clonogenic survival was described as the number of colony-forming units in treated cultures in comparison to untreated controls.

AUTHOR INFORMATION

Corresponding Authors

Vijay Kumar − *Department of Physics, National Institute of Technology (NIT), Srinagar 190006, Jammu and Kashmir, India*; orcid.org/0000-0002-7438-8496; Email: vj.physics@gmail.com

Vishal Sharma − *Institute of Forensic Science & Criminology, Panjab University, Chandigarh 160014, India*; Email: vsharma@pu.ac.in

Authors

Kashma Sharma − *Institute of Forensic Science & Criminology, Panjab University, Chandigarh 160014, India*

Shreya Sharma − *Institute of Forensic Science & Criminology, Panjab University, Chandigarh 160014, India*

Sonia Thapa − *Cancer Pharmacology Division, CSIR-IIIM, Jammu 180001, Jammu and Kashmir, India*

Madhulika Bhagat − *School of Biotechnology, University of Jammu, Jammu 180006, Jammu and Kashmir, India*

Complete contact information is available at: https://pubs.acs.org/10.1021/acsomega.0c03125

Notes

The authors declare no competing financial interest.

https://dx.doi.org/10.1021/acsomega.0c03125
ACS Omega 2020, 5, 27886−27895

■ ACKNOWLEDGMENTS

One of the authors, K.S., is grateful to the University Grants Commission (UGC), New Delhi, India, for providing Postdoctoral Fellowship for Women [F.15-1/2017/PDFWM-2017-18-HIM-51703(SA-II)] to carry out the research. The authors (K.S. and V.K.) also acknowledge the Indo-US Science and Technology Forum for the support through grant no. IUSSTF/JC-025/2016.

■ REFERENCES

(1) Edelstein, B. The Dental Caries Pandemic and Disparities Problem. *BMC Oral Health* **2006**, *6*, S2.
(2) Wu, Y.-R.; Chang, C.-W.; Ko, C.-L.; Wu, H.-Y.; Chen, W.-C. The morphological effect of calcium phosphates as reinforcement in methacrylate-based dental composite resins on mechanical strength through thermal cycling. *Ceram. Int.* **2017**, *43*, 14389−14394.
(3) Abou Neel, E. A.; Aljabo, A.; Strange, A.; Ibrahim, S.; Coathup, M.; Young, A. M.; Bozec, L.; Mudera, V. Demineralization-remineralization dynamics in teeth and bone. *Int. J. Nanomed.* **2016**, *11*, 4743−4763.
(4) Marsh, P. D. Dental plaque as a biofilm and a microbial community − implications for health and disease. *BMC Oral Health* **2006**, *6*, S14.
(5) Drachev, S. N.; Brenn, T.; Trovik, T. A. Dental caries experience and determinants in young adults of the Northern State Medical University, Arkhangelsk, North-West Russia: a cross-sectional study. *BMC Oral Health* **2017**, *17*, 136.
(6) Kojima, A.; Ekuni, D.; Mizutani, S.; Furuta, M.; Irie, K.; Azuma, T.; Tomofuji, T.; Iwasaki, Y.; Morita, M. Relationships between self-rated oral health, subjective symptoms, oral health behavior and clinical conditions in Japanese university students: a cross-sectional survey at Okayama University. *BMC Oral Health.* **2013**, *13*, 62.
(7) Kaidonis, J.; Townsend, G. The 'sialo−microbial−dental complex' in oral health and disease. *Ann. Anat.* **2016**, *203*, 85−89.
(8) Sebastian, A.; Frassetto, L. A.; Sellmeyer, D. E.; Merriam, R. L.; Morris, R. C., Jr. Estimation of the net acid load of the diet of ancestral preagricultural Homo sapiens and their hominid ancestors. *Am. J. Clin. Nutr.* **2002**, *76*, 1308−1316.
(9) Adler, C. J.; Dobney, K.; Weyrich, L. S.; Kaidonis, J.; Walker, A. W.; Haak, W.; Bradshaw, C. J. A.; Townsend, G.; Sołtysiak, A.; Alt, K. W.; Parkhill, K.; Cooper, A. Sequencing ancient calcified dental plaque shows changes in oral microbiota with dietary shifts of the Neolithic and Industrial revolutions. *Nat. Genet.* **2013**, *45*, 450−455.
(10) Hench, L. L. Bioceramics: from concept to clinic. *J. Am. Ceram. Soc.* **1991**, *74*, 1487−1510.
(11) Chevalier, J.; Gremillard, L. Ceramics for medical applications: a picture for the next 20 years. *J. Eur. Ceram. Soc.* **2009**, *29*, 1245−1255.
(12) Dorozhkin, S. V. Calcium orthophosphate bioceramics. *Ceram. Int.* **2015**, *41*, 13913−13966.
(13) Montalbano, G.; Molino, G.; Fiorilli, S.; Vitale-Brovarone, C. Synthesis and incorporation of rod-like nano-hydroxyapatite into type I collagen matrix: A hybrid formulation for 3D printing of bone scaffolds. *J. Eur. Ceram. Soc.* **2020**, *40*, 3689−3697.
(14) Habelitz, S.; Marshall, S. J.; Marshall, G. W., Jr.; Balooch, M. Mechanical properties of human dental enamel on the nanometre scale. *Arch. Oral Biol.* **2001**, *46*, 173−183.
(15) Zaharia, A.; Muşat, V.; Anghel, E. M.; Atkinson, I.; Mocioiu, O. C.; Buşilă, M.; Pleşcan, V. G. Biomimetic chitosan-hydroxyapatite hybrid biocoatings for enamel remineralization. *Ceram. Int.* **2017**, *43*, 11390−11402.
(16) Ayoub, G.; Veljovic, D.; Zebic, M. L.; Miletic, V.; Palcevskis, E.; Petrovic, R.; Janackovic, D. Composite nanostructured hydroxyapatite/yttrium stabilized zirconia dental inserts − The processing and application as dentin substitutes. *Ceram. Int.* **2018**, *44*, 18200−18208.
(17) Zhou, H.; Lee, J. Nanoscale hydroxyapatite particles for bone tissue engineering. *Acta Biomater.* **2011**, *7*, 2769−2781.
(18) Schliephake, H.; Neukam, F. W.; Klosa, D. Influence of pore dimensions on bone ingrowth into porous hydroxyapatite blocks used as bone graft substitutes: A histometric study. *Int. J. Oral Maxillofac. Surg.* **1991**, *20*, 53−58.
(19) Okumura, M.; Ohgushi, H.; Dohi, Y.; Katuda, T.; Tamai, S.; Koerten, H. K.; Tabata, S. Osteoblastic phenotype expression on the surface of hydroxyapatite ceramics. *J. Biomed. Mater. Res.* **1997**, *37*, 122−129.
(20) Jansen, J. A.; Wolke, J. G. C.; Swann, S.; Van der Waerden, J. C. P. M.; de Groot, K. Application of magnetron sputtering for the producing ceramic coatings on implant materials. *Clin. Oral Implant Res.* **1993**, *4*, 28−34.
(21) Blind, O.; Klein, L. H.; Dailey, B.; Jordan, L. Characterization of hydroxyapatite films obtained by pulsed-laser deposition on Ti and Ti-6AL-4v substrates. *Dent. Mater.* **2005**, *21*, 1017−1024.
(22) Sugawara, A.; Kusama, K.; Nishimura, S.; Nishiyama, M.; Moro, I.; Kudo, I.; Takagi, S. Histopathological reaction of a calcium phosphate cement root canal filler. *J. Hard Tissue Biol.* **1995**, *4*, 1−7.
(23) Cherng, A. M.; Chow, L. C.; Takagi, S. In vitro evaluation of a calcium phosphate cement root canal filler/sealer. *J. Endodontics* **2001**, *27*, 613−615.
(24) Dickens-Venz, S. H.; Takagi, S.; Chow, L. C.; Bowen, R. L.; Johnston, A. D.; Dickens, B. Physical and chemical properties of resin-reinforced calcium phosphate cements. *Dent. Mater.* **1994**, *10*, 100−106.
(25) Dickens, S. H.; Flaim, G. M.; Takagi, S. Mechanical properties and biochemical activity of remineralizing resin-based Ca-PO4 cements. *Dent. Mater.* **2003**, *19*, 558−566.
(26) Bayne, S. C.; Thompson, J. Y.; Swift, E. J., Jr.; Stamatiades, P.; Wilkerson, M. A characterization of first-generation flowable composites. *J. Am. Dent Assoc.* **1998**, *129*, 567−577.
(27) Ferracane, J. L.; Berge, H. X.; Condon, J. R. In vitro aging of dental composites in water—effect of degree of conversion, filler volume, and filler/matrix coupling. *J. Biomed. Mater. Res.* **1998**, *42*, 465−472.
(28) Watts, D. C.; Hindi, A. A. Intrinsic "soft-start" polymerization shrinkage-kinetics in an acrylate-based resin composite. *Dent. Mater.* **1999**, *15*, 39−45.
(29) Domingo, C.; Arcís, R. W.; Osorio, E.; Osorio, R.; Fanovich, M. A.; Rodríguez-Clemente, R.; Toledano, M. Hydrolytic stability of experimental hydroxyapatite-filled dental composite materials. *Dent. Mater.* **2003**, *19*, 478−486.
(30) Bryington, M. S.; Hayashi, M.; Kozai, Y.; Vandeweghe, S.; Andersson, M.; Wennerberg, A.; Jimbo, R. The influence of nano hydroxyapatite coating on osseointegration after extended healing periods. *Dent. Mater.* **2013**, *29*, 514−520.
(31) Tschoppe, P.; Zandim, D. L.; Martus, P.; Kielbassa, A. M. Enamel and dentine remineralization by nano-hydroxyapatite toothpastes. *J. Dent.* **2011**, *39*, 430−437.
(32) Nozari, A.; Ajami, S.; Rafiei, A.; Niazi, E. Impact of Nano Hydroxyapatite, Nano Silver Fluoride and Sodium Fluoride Varnish on Primary Teeth Enamel Remineralization: An In Vitro Study. *J. Clin. Diagn. Res.* **2017**, *9*, ZC97−ZC100.
(33) Sharma, K.; Sharma, S.; Kaur Bhatia, J.; Sharma, V.; Kumar, V. Methylene blue dye adsorption with Au-NPs impregnated nano-hydroxyapatite: A kinetics and equilibrium studies with the use of dye adsorbed waste in antibacterial application, Submitted 2020.
(34) Su, K.; Wang, C. Recent advances in the use of gelatin in biomedical research. *Biotech. Lett.* **2015**, *37*, 2139−2145.
(35) Rungsiyanont, S.; Dhanesuan, N.; Swasdison, S.; Kasugai, S. Evaluation of biomimetic scaffold of gelatin-hydroxyapatite crosslink as a novel scaffold for tissue engineering: biocompatibility evaluation with human PDL fibroblasts, human mesenchymal stromal cells, and primary bone cells. *J. Biomat. Appl.* **2012**, *27*, 47−54.
(36) Dressler, M.; Dombrowski, F.; Simon, U.; Börnstein, J.; Hodoroaba, V. D.; Feigl, M.; Grunow, S.; Gildenhaar, R.; Neumann, M. Influence of gelatin coatings on compressive strength of porous hydroxyapatite ceramics. *J. Eur. Ceram. Soc.* **2011**, *31*, 523−529.

https://dx.doi.org/10.1021/acsomega.0c03125
ACS Omega 2020, 5, 27886−27895

(37) Mohammadinejad, R.; Maleki, H.; Larrañeta, E.; Fajardo, A. R.; Nike, A. B.; Shavandi, A.; Sheikh, A.; Ghorbanpour, M.; Farokhi, M.; Govindh, P.; Cabane, E.; Azizi, S.; Aref, A. R.; Mozafari, M.; Mehrali, M.; Thomas, S.; Mano, J. F.; Mishra, Y. K.; Thakur, V. K. Status and future scope of plant-based green hydrogels in biomedical engineering. *Appl. Mater. Today* **2019**, *16*, 213−246.
(38) Gutekunst, S. B.; Siemsen, K.; Huth, S.; Möhring, A.; Hesseler, B.; Timmermann, M.; Paulowicz, I.; Mishra, Y. K.; Siebert, L.; Adelung, R.; Selhuber-Unkel, C. 3D Hydrogels Containing Interconnected Microchannels of Subcellular Size for Capturing Human Pathogenic Acanthamoeba Castellanii. *ACS Biomater. Sci. Eng.* **2019**, *5*, 1784−1792.
(39) Sobczak-Kupiec, A.; Malina, D.; Piatkowski, M.; Krupa-Zuczek, K.; Wzorek, Z.; Tyliszczak, B. Physicochemical and biological properties of hydrogel/gelatin/hydroxyapatite PAA/G/HAp/AgNPs composites modified with silver nanoparticles. *J. Nanosci. Nanotech.* **2012**, *12*, 9302−9311.
(40) Mohd Pu'ad, N. A. S.; Koshy, P.; Abdullah, H. Z.; Idris, M. I.; Lee, T. C. Syntheses of hydroxyapatite from natural sources. *Heliyon* **2019**, *5*, No. e01588.
(41) Carniti, P.; Gervasini, A.; Tiozzo, C.; Guidotti, M. Niobium-Containing Hydroxyapatites as Amphoteric Catalysts: Synthesis, Properties, and Activity. *ACS Catal.* **2014**, *4*, 469−479.
(42) Bouyarmane, H.; El Asri, S.; Rami, A.; Roux, C.; Mahly, M. A.; Saoiabi, A.; Coradin, T.; Laghzizil, A. Pyridine and Phenol Removal Using Natural and Synthetic Apatites as Low Cost sorbents: Influence of Porosity and Surface Interactions. *J. Hazard. Mater.* **2010**, *181*, 736−741.
(43) Pezzotti, G.; Asmus, S. M. F. Fracture behavior of hydroxyapatite/polymer interpenetrating network composites prepared by in situ polymerization process. *Mater. Sci. Engg.* **2001**, *316*, 231−237.
(44) Siahrostami, S.; Li, G.-L.; Viswanathan, V.; Nørskov, J. K. One- or Two-Electron Water Oxidation, Hydroxyl Radical, or H2O2 Evolution. *J. Phys. Chem. Lett.* **2017**, *8*, 1157−1160.
(45) Bedwell, S.; Dean, R. T.; Jessup, W. The action of defined oxygen-centred free radicals on human low-density lipoprotein. *Biochem. J.* **1989**, *262*, 707−712.
(46) Zhang, H. J.; Wang, L.; Wang, X.; Han, Q.; You, X. Developing Super Tough Gelatin-based Hydrogels by Incorporating Linear Poly(methacrylic Acid) to Facilitate Sacrificial Hydrogen Bonding. *Soft Matter* **2020**, *16*, 4723−4727.
(47) Hu, X.; Vatankhah-Varnoosfaderani, M.; Zhou, J.; Li, Q.; Sheiko, S. S. Weak Hydrogen Bonding Enables Hard, Strong, Tough, and Elastic Hydrogels. *Adv. Mater.* **2015**, *27*, 6899−6905.
(48) Zhang, H. J.; Sun, T. L.; Zhang, A. K.; Ikura, Y.; Nakajima, T.; Nonoyama, T.; Kurokawa, T.; Ito, O.; Ishitobi, H.; Gong, J. P. Tough Physical Double-Network Hydrogels Based on Amphiphilic Triblock Copolymers. *Adv. Mater.* **2016**, *28*, 4884−4890.
(49) Rokaya, D.; Srimaneepong, V.; Sapkota, J.; Qin, J.; Siraleartmukul, K.; Siriwongrungson, V. Polymeric materials and films in dentistry: An overview. *J. Adv. Res.* **2018**, *14*, 25−34.
(50) Fornell, A. C.; Sköld-Larsson, K.; Hallgren, A.; Bergstand, F.; Twetman, S. Effect of a hydrophobic tooth coating on gingival health, mutans streptococci, and enamel demineralization in adolescents with fixed orthodontic appliances. *Acta. Odontol. Scand.* **2002**, *60*, 37−41.
(51) Peroglio, M.; Gremillard, L.; Chevalier, J.; Chazeau, L.; Gauthier, C.; Hamaide, T. Toughening of bio-ceramics scaffolds by polymer coating. *J. Eur. Ceram. Soc.* **2007**, *27*, 2679−2685.
(52) Nasiri-Tabrizin, B.; Fahami, A. Mechanochemical synthesis and structural characterization of nano-sized amorphous tricalcium phosphate. *Ceram. Int.* **2013**, *39*, 8657−8666.
(53) Nasiri-Tabrizi, B.; Fahami, A.; Ebrahimi-Kahrizsangi, R. Effect of milling parameters on the formation of nanocrystalline hydroxyapatite using different raw materials. *Ceram. Int.* **2013**, *39*, 5751−5763.
(54) Manda, M.; Goudouri, O. M.; Papadopoulou, L.; Kantiranis, N.; Christofilos, D.; Triantafyllidis, K.; Paraskevopoulos, K. M.; Koidis, P. Material characterization and bioactivity evaluation of dental porcelain modified by bioactive glass. *Ceram. Int.* **2012**, *38*, 5585−5596.
(55) Sharma, K.; Kumar, V.; Swart-Pistor, C.; Chaudhary, B.; Swart, H. C. Synthesis, characterization, and anti-microbial activity of superabsorbents based on agar−poly(methacrylic acid-glycine). *J. Bioact. Compat. Polym.* **2016**, *32*, 1−91.
(56) Adeogun, A. I.; Ofudje, E. A.; Idowu, M. A.; Kareem, S. O.; Vahidhabanu, S.; Babu, B. R. Biowaste-Derived Hydroxyapatite for Effective Removal of Reactive Yellow 4 Dye: Equilibrium, Kinetic, and Thermodynamic Studies. *ACS Omega* **2018**, *3*, 1991−2000.
(57) Varaprasad, K.; Nunez, D.; Yallapu, M. M.; Jayaramudu, T.; Elgueta, E.; Oyarzun, P. Nano-hydroxyapatite polymeric hydrogels for dye Removal. *RSC Adv.* **2018**, *8*, 18118−18127.
(58) Wu, X.; Liu, Y.; Wang, W.; Han, Y.; Liu, A. Improved mechanical and thermal properties of gelatin films using a nano inorganic filler. *J. Food Process Eng.* **2017**, *40*, No. e12469.
(59) Anusha Thampi, V. V.; Prabhu, M.; Kavitha, K.; Manivasakan, P.; Prabu, P.; Rajendran, V.; Shankar, S.; Kulandaivelu, P. Hydroxyapatite, alumina/zirconia, and nanobioactive glass cement for tooth-restoring applications. *Ceram. Int.* **2014**, *40*, 14355−14365.
(60) Zamanian, A.; Yasaei, M.; Ghaffari, M.; Mozafari, M. Calcium hydroxide-modified zinc polycarboxylate dental cements. *Ceram. Int.* **2013**, *39*, 9525−9532.
(61) Loesche, W. J. Role of Sterptocococcus mutans in human dental decay. *Microbiol. Rev.* **1986**, *50*, 353−380.
(62) Minguez, F.; Agra, M.; Luruena, S.; Ramos, C.; Prieto, J. Post-antibiotic effect of isepamicin compared to that of other aminoglycosides. *Drugs Exp. Clin. Res.* **1990**, *16*, 231−235.
(63) Pepla, E.; Besherat, L. K.; Palaia, G.; Tenore, G.; Migliau, G. Nano-hydroxyapatite and its applications in preventive, restorative and regenerative dentistry: a review of literature. *Ann. Stomatol.* **2014**, *3*, 108−114.
(64) Xu, Z. L.; Sun, J.; Liu, C. S.; Wei, J. Effect of hydroxyapatite nanoparticles of different concentrations on rat osteoblast. *Mater. Sci. Forum* **2009**, *610-613*, 1364−1369.
(65) Kim, H.-W.; Kim, H.-E.; Salih, V. Stimulation of osteoblast responses to biomimetic nanocomposites of gelatin−hydroxyapatite for tissue engineering scaffolds. *Biomaterials* **2005**, *26*, 5221−5230.
(66) Sumantran, V. N.; Boddul, S.; Koppikar, S. J.; Dalvi, M.; Wele, A.; Gaire, V.; Wagh, U. V. Differential growth inhibitory effects of W. somnifera root and E. officinalis fruits on CHO cells. *Phytother. Res.* **2007**, *21*, 496−499.
(67) Saotome, K.; Morita, H.; Umeda, M. Cytotoxicity test with simplified crystal violet staining method using microtitre plates and its application to injection drugs. *Toxicol. In Vitro* **1989**, *3*, 317−321.
(68) Webster, T. J.; Ergun, C.; Doremus, R. H.; Siegel, R. W.; Bizios, R. Specific proteins mediate enhanced osteoblast adhesion on nanophase ceramics. *J. Biomed. Mater. Res. A* **2000**, *51*, 475−483.
(69) Hassan, S. E.-D.; Fouda, A.; Radwan, A. A.; Salem, S. S.; Barghoth, M. G.; Awad, M. A.; Abdo, A. M.; El-Gamal, M. S. Endophytic actinomycetes Streptomyces spp mediated biosynthesis of copper oxide nanoparticles as a promising tool for biotechnological applications. *J. Biol. Inorg. Chem.* **2019**, *24*, 377−393.
(70) Li, L. H.; Kong, Y. M.; Kim, H. W.; Kim, Y. W.; Kim, H. E.; Heo, S. J.; Koak, J. Y. Improved biological performance of Ti implants due to surface modification by micro-arc oxidation. *Biomaterials* **2004**, *25*, 2867−2875.
(71) Linez-Bataillon, P.; Monchau, F.; Bigerelle, M.; Hildebrand, H. F. In vitro MC3T3 osteoblast adhesion with respect to surface roughness of Ti6Al4V substrates. *Biomol. Eng.* **2002**, *19*, 133−141.
(72) Gupta, N.; Rath, S. K.; Singh, J.; Qayum, A.; Singh, S.; Sangwan, P. L. Synthesis of novel benzylidene analogues of betulinic acid as potent cytotoxic agent. *Europ. J. Med. Chem.* **2017**, *135*, 517−530.
(73) Godwin, M. A.; Mahithashri, K.; Shiney, O. J.; Bhagat, M.; Praseetha, P. K. Metal incorporated g-C_3N_4 nanosheets as potential cytotoxic agents for promoting free radical scavenging in Cancer Cell Lines. *J. Nanosci. Nanotechnol.* **2019**, *19*, 5448−5455.

https://dx.doi.org/10.1021/acsomega.0c03125
ACS Omega 2020, 5, 27886−27895